C. T.-C. Nguyen, “Vibrating RF MEMS for next generation wireless applications,” *Proceedings*, 2004 IEEE Custom Integrated Circuits Conf., Orlando, Florida, Oct. 3-6, 2004, pp. 257-264.

Vibrating RF MEMS for Next Generation Wireless Applications

Clark T.-C. Nguyen

Center for Wireless Integrated Micro Systems (WIMS)
Dept. of EECS, University of Michigan
Ann Arbor, Michigan 48109-2122, U.S.A.
Email: ctnguyen@eecs.umich.edu

Abstract

Micromechanical RF filters and reference oscillators based on recently demonstrated vibrating on-chip micromechanical resonators with Q’s >10,000 at 1.5 GHz, are described as an attractive solution to the increasing count of RF components (e.g., filters) expected to be needed by future multi-band wireless devices. With Q’s this high in on-chip abundance, such devices might also enable a paradigm-shift in transceiver design where the advantages of high-Q are emphasized, rather than suppressed, resulting in enhanced robustness and power savings. An overview of the latest in vibrating RF MEMS technology is presented with an addendum on remaining issues to be addressed for insertion into tomorrow’s handsets.

Introduction

Today’s wireless transceivers are generally designed under a near mandate to minimize or eliminate, in as much as possible, the use of high-Q passives. The reasons for this are quite simple: cost and size. Specifically, the ceramic filters, SAW filters, quartz crystals, and now FBAR filters, capable of achieving the Q’s from 500-10,000 needed for RF and IF bandpass filtering, and frequency generation functions, are all off-chip components that must interface with transistor functions at the board-level, taking up a sizable amount of the total board volume, and comprising a sizable fraction of the parts and assembly cost.

Pursuant to reducing the off-chip parts count in modern cellular handsets, direct-conversion receiver architectures [1] have removed the IF filter, and integrated inductor technologies are removing some of the off-chip L’s used for bias and matching networks [2]. Although these methods can lower cost, they often do so at the expense of increased transistor circuit complexity and more stringent requirements on circuit performance (e.g., dynamic range), both of which degrade somewhat the robustness and power efficiency of the overall system. In addition, the removal of the IF filter does little to appease the impending needs of future multi-band reconfigurable handsets that will likely require high-Q RF filters in even larger quantities—perhaps one set for each wireless standard to be addressed. Fig. 1 compares the simplified system block diagram for a present-day handset receiver with one targeted for multi-band applications, clearly showing that it is the high-Q RF filters, not the IF filter, that must be addressed. In the face of this need, an option to reinsert high Q components without the size and cost penalties of the past would be most welcome.

Recent advances in vibrating RF microelectromechanical systems (“MEMS”) technology that have yielded on-chip resonators operating past GHz frequencies with Q’s in excess of 10,000, may now not only provide an attractive solution to the above, but might also enable a paradigm-shift in transceiver design where the advantages of high-Q (e.g., in filters and oscillators) are emphasized, rather than suppressed [3][4]. In particular, like transistors, micromechanical elements can be used in large quantities without adding significant cost. This not only brings more robust superheterodyne architectures back into contention, but also encourages modifications to take advantage of a new abundance in low loss ultra-high-Q frequency shaping at GHz frequencies. For example, an RF channel-select filter bank may now be possible, capable of eliminating not only out-of-band interferers, but also out-of-channel interferers, and in so doing, relaxing the dynamic range requirements of the LNA and mixer, and the phase noise requirements

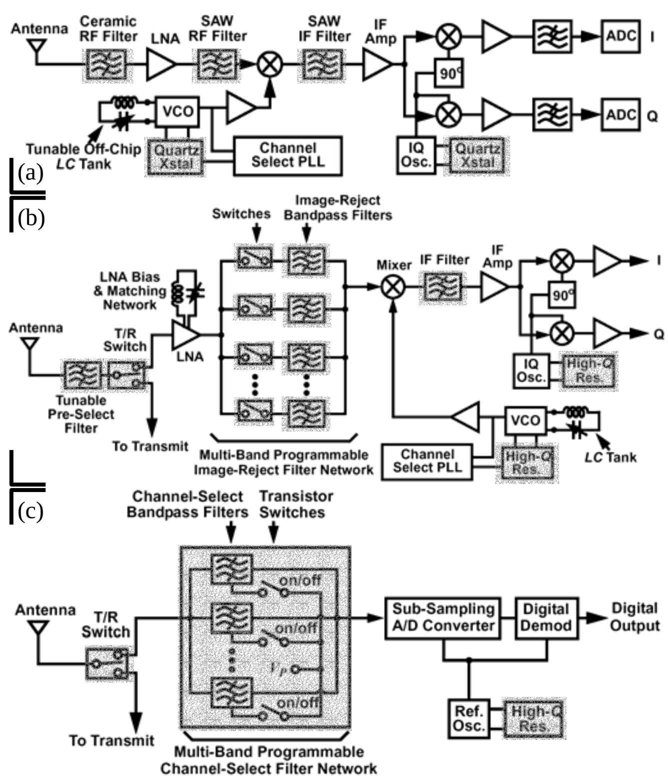

Fig. 1: Expected progression of transceiver front-end architectures when vibrating RF MEMS (shaded) are employed. (a) Present-day superheterodyne. (b) Multi-band architecture, where the number of RF filters could reach >10. (c) Highly reconfigurable, low-power, RF channel-select architecture, where the number of RF filters could reach >100.

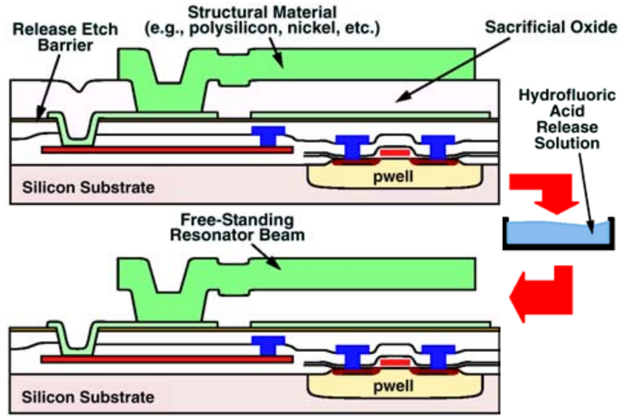

Fig. 2: Cross-sections (a) immediately before and (b) after release of a surface-micromachining process done directly over CMOS [5].

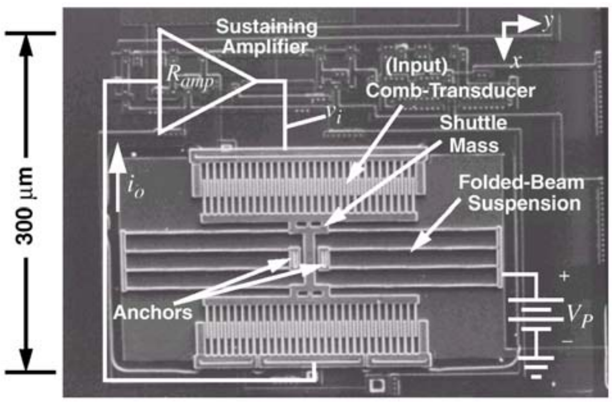

Fig. 3: SEM of a fully integrated watch oscillator that combines CMOS and MEMS in a single fully planar process [5].

of the local oscillator, to the point of perhaps allowing complete transceiver implementations using very low cost transistor circuits (e.g., perhaps eventually even organic circuits).

MEMS Technology

There are now a wide array of MEMS technologies capable of attaining on-chip micro-scale mechanical structures, each distinguishable by not only the type of starting or structural material used (e.g., silicon, silicon carbide, glass, plastic, etc.), but also by the method of micromachining (e.g., surface, bulk, 3D growth, etc.), and by the application space (e.g., optical MEMS, bio MEMS, etc.). For the present focus on portable communications, MEMS technologies amenable to low capacitance merging of micromechanical structures together with integrated transistor circuits are of most interest. In this regard, surface micromachining technologies, where structural materials are obtained exclusively via deposition processes, are perhaps most applicable to the present discussion.

Fig. 2 presents key cross-sections describing a polysilicon surface micromachining process done directly over silicon CMOS circuits. As shown, this process entails depositing and patterning films above the CMOS circuits using the same equipments already found in CMOS foundries until a cross section as in Fig. 2(a) is achieved. Here, the structural polysilicon layer has been temporarily supported by a sacrificial oxide film during its own deposition and patterning. After achieving the cross-section of Fig. 2(a), the whole wafer is dipped into an isotropic etchant, in this case hydrofluoric acid, which attacks only the oxide sacrificial layer, removing it and leaving the structural polysilicon layer intact, free to move in multiple dimensions. Fig. 3 presents the SEM of a watch oscillator that combines a 16 kHz folded-beam micromechanical resonator with sustaining CMOS transistor circuits using this very process flow, but with tungsten as the metal interconnect in order to accommodate 625^o structural polysilicon deposition temperatures [5].

Vibrating Micromechanical Resonators

A major impetus behind MEMS technology stems from the fact that mechanical mechanisms benefit from the same scaling-based advantages that have driven the integrated circuit (IC) revolution in recent decades. Specifically, small size leads to faster speed, lower power consumption, higher complexity, and lower cost. And it does so not only in the electrical domain, but in virtually all other domains, including and especially mechanical. Although many examples of this from all physical domains exist, vibrating RF MEMS resonators perhaps provide the most direct example of how small size leads to faster speed in the mechanical domain.

For example, on the macro-scale, a guitar string made of nickel and steel, spanning about 25” in length, and tuned to a musical “A” note, will vibrate at a resonance frequency of 110 Hz when plucked. In vibrating only at 110 Hz, and no other frequency, this guitar string is actually mechanically selecting this frequency, and is doing so with a Q on the order of 350, which is ~50X more frequency selective than an on-chip electrical LC tank. Of course, selecting a frequency like this is exactly what the RF and IF filters of a wireless phone must do, except they must do so at much higher frequencies, from tens of MHz to well into the GHz range. To achieve such frequencies with even better mechanical selectivities, dimensional scaling is needed. In particular, by shrinking a guitar string from 25” down to only 10μm, constructing it in stiffer, IC-compatible materials (like polysilicon), supporting it at nodes rather than at its ends (to minimize anchor losses), and exciting it electrostatically or piezoelectrically rather than plucking it, one can achieve a free-free beam (“FF-beam) resonator such as summarized in row 2 of Table 1 that resonates at frequencies around 100 MHz with Q’s in excess of 10,000 [6][7].

In keeping with the scaling-based arguments presented so far, further scaling down to nano-dimensions does indeed yield frequencies in excess of 1 GHz [8]. However, as with nanoelectronics in the electrical domain, there are issues in the mechanical domain that might hinder the use of nanomechanical vibrating resonators (at least in their present form) for today’s communication purposes. In particular, excessive scaling may lead to “scaling-induced limitations”, such as adsorption-desorption noise [9], temperature fluctuation noise, and insufficient power handling, with the last of these perhaps being the most serious for present day applications. As with nanoelectronics, the power handling issue with nanomechanical resonators really boils down to an impedance matching problem. In brief, nanostructures would rather operate at higher impedance levels than macroscopic counterparts, and in order to interface

Table 1: Vibrating RF MEMS Resonators Most Useful for Communications

Device	Photo	Performance	Applications	Research Issues
CC-Beam Resonator [17]	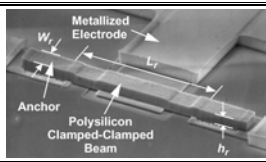	Demo'ed: Q ~8,000 @ 10MHz (vac) Q ~50 @ 10MHz (air) Q ~300 @ 70MHz (anchor diss.) Q drop w/ freq. limits freq. range Series Resistance, R_x ~5-5,000Ω	Reference Oscillator HF-VHF Filter HF-VHF Mixer-Filter (arrays of the above)	power handling thermal/aging stability impedance vacuum packaging
FF-Beam Resonator [6]	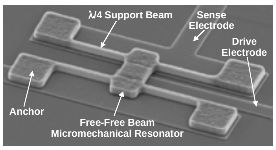	Demo'ed: Q ~20,000 from 10-200 MHz Q ~2,000 @ 90 MHz (air) No drop in Q with freq. Freq. Range: >1GHz; unlimited w/ scaling and use of higher modes Series Resistance, R_x ~5-5,000Ω	Reference Oscillator HF-UHF Filter HF-UHF Mixer-Filter Ka-Band? (arrays of above)	freq. extension power handling thermal/aging stability impedance vacuum packaging
Wine-Glass Disk Res. [21]	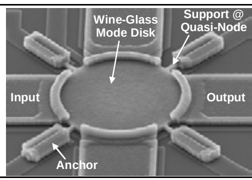	Demo'ed: Q ~156,000 @ 60 MHz (vac) Q ~8,000 @ 98 MHz (air) Perimeter support design nulls anchor loss to allow extremely high Q Freq. Range: >1GHz; unlimited w/ scaling Series Resistance, R_x ~5-5,000Ω	Reference Oscllator HF-UHF Filter HF-UHF Mixer-Filter (arrays of the above)	freq. extension power handling thermal/aging stability impedance
Contour-Mode Disk Res. [11]	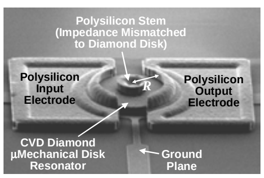	Demo'ed: Q ~11,555 @ 1.5 GHz (vac) Q ~10,100 @ 1.5 GHz (air) Balanced design and material mismatching anchor-disk design nulls anchor loss Freq. Range: >1GHz; unlimited w/ scaling and use of higher modes Series Resistance, R_x ~50-50,000Ω	RF Local Oscillator VHF-S-Band Filter VHF-S-Band Mixler Ka-Band? RF Channel-Select (arrays of above)	thermal/aging stability impedance Xmit power handling
Hollow Disk Ring Res. [12]	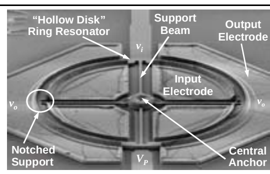	Demo'ed: Q ~14,600 @ 1.2 GHz (vac) λ/4 support design nulls anchor loss Freq. Range: >1GHz; unlimited w/ scaling and use of higher modes Series Resistance, R_x ~50-5,000Ω	RF Local Oscillator UHF-S-Band Filter UHF-S-Band Mixler Ka-Band? RF Channel-Select (arrays of above)	thermal/aging stability impedance Xmit power handling

the nano with the macro (e.g., the antenna), impedance matching strategies like massive arraying of nanostructures to add their responses might be required.

Fortunately, massive-scale arraying isn't really needed, at least not for the frequency range used by present day commercial wireless standards. In particular, GHz frequencies can be attained mechanically without the need for nano-scale dimensions, and thus, without its associated power handling issues, by merely using alternative resonator geometries that operate in modes more amenable to higher frequency. Row 4 of Table 1 presents the SEM and characteristics of one such device demonstrated very recently: A 1.51-GHz radial-contour mode vibrating micromechanical disk exhibiting a record (at this frequency) room temperature Q of 11,555 in vacuum, and 10,100 in air. As shown, this resonator consists of a polydiamond disk suspended by a polysilicon stem at its very center, and completely surrounded by polysilicon electrodes spaced less than 100 nm from its outer perimeter capable of electrostatically driving the disk into a mode shape where it expands and contracts along its radius, in a motion reminiscent of breathing [10][11]. The astonishingly high Q at greater than GHz frequencies is a result of the sheer symmetry of this disk design, and of a strategic impedance-mismatch between the polydiamond disk and polysilicon stem, both of which greatly suppress energy loss through the disk anchor [11]. Since the resonance frequency of this device goes approximately as the inverse of its radius, even higher frequency (>10 GHz) with similar Q's is expected through radial scaling and the use of higher radial modes.

As detailed in [11], the use diamond as the structural material for the radial mode resonator of row 4 in Table 1 contributes to the ease with which it achieves high frequency, since diamond's acoustic velocity is twice that of silicon. However, diamond is not necessary to achieve Q's greater than 10,000 at frequencies past 1 GHz. Rather, as long as a properly impedance-mismatched resonator-to-anchor transition can be attained, polysilicon also works well, as demonstrated by a recent "hollow disk" extensional-mode ring resonator, shown in row 5 of Table 1. This device uses a centrally located support structure, attached to the ring at notched nodal locations and designed with dimensions corresponding to a quarter-wavelength of the ring resonance frequency, in order to reflect vibrational energy away from the central anchor and back into the ring. The ring itself vibrates extensionally by expanding and contracting along its inner and outer perimeter edges in a mode shape that allows very high frequency. With this design strategy, this polysilicon ring resonator achieves a Q of 14,603 at 1.2 GHz, which is the highest Q to date past 1 GHz for any on-chip resonator at room temperature [12][13][14]. The device is amenable to much higher frequency, as well, with a resonance fre-

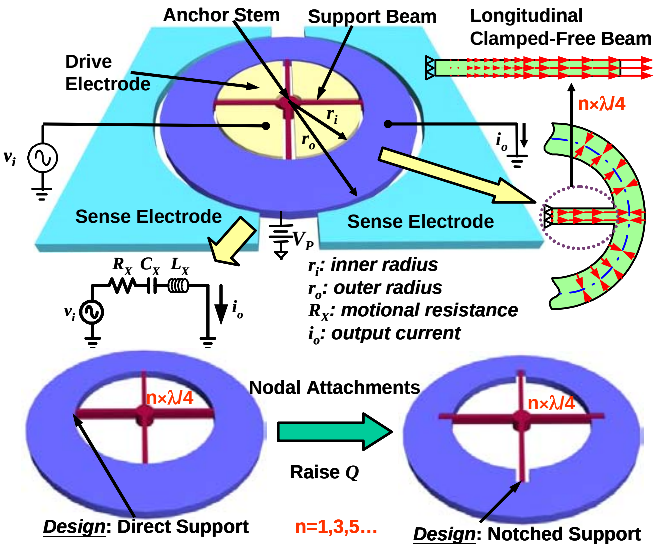

Fig. 4: Perspective-view schematic summarizing the design and operation of the "hollow disk" ring resonator of row 5 in Table 1, and emphasizing the importance of λ/4 support design and notched support-to-ring attachment locations to maximize *Q*.

quency determined primarily by the width of the ring.

Pursuant to better specifying the operation mode for these devices, Fig. 1 presents a clearer perspective-view schematic of the "hollow disk" ring of row 5 in Table 1, indicating key features, and specifying the required electrical input and output configuration for capacitively transduced operation. As shown, under normal operation, the mechanical structure must be charged, in this case via dc-bias voltage V_P (from which no dc current flows once the conductive structure is charged, so there is no dc power consumption). Alternatively a charge can be placed on the structure itself (e.g., by implantation) to effectively realize an electret that obviates the need for a voltage source. The voltage V_P generated by the charge effectively amplifies both the force imposed by the ac excitation signal v_i and the output motional current i_o generated by the dc-biased time-varying electrode-to-resonator capacitor that results when the ring vibrates. The transfer function from input to short-circuited output can be expressed as

$$\frac{i_o}{v_i}(s) = \frac{1}{R_x}\frac{(\omega_o/Q)s}{s^2 + (\omega_o/Q)s + \omega_o^2} \quad (1)$$

where ω_o is its radian resonance frequency, and R_x is the series motional resistance of the device, given by

$$R_x = \frac{m_r k_r}{Q}\frac{1}{V_P^2}\left[\frac{\varepsilon_o}{d_o^2}\right]^2 A_i A_o = \frac{m_r k_r}{Q}\frac{1}{V_P^2}\left[\frac{2\pi\varepsilon_o h}{d_o^2}\right]^2 r_i r_o \quad (2)$$

where m_r and k_r are the equivalent mass and stiffness of the resonator ring, respectively; ε_o is the permittivity in vacuum; h is the ring thickness; d_o is the electrode-to-resonator gap spacing; A_i and A_o are the inner and outer electrode-to-resonator overlap areas, respectively; and r_i and r_o are the inner and outer ring radii, respectively, defined in Fig. 4. Recognizing (1) as the transfer function for a classic bandpass biquad, the micromechanical resonator of Fig. 4, and virtually all two-port vibrating mechanical resonators, can be modeled by the equivalent *LCR* electrical circuit shown in the figure.

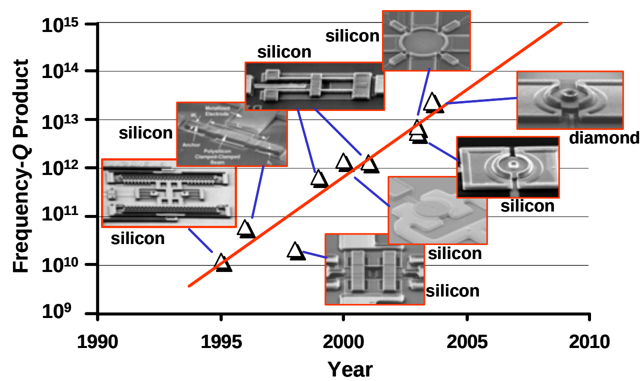

Fig. 5: Plot showing exponential growth in the frequency-*Q* product of micromechanical resonators over time.

Fig. 5 presents a graph showing how the frequency-*Q* product, a common figure of merit for resonators, has increased exponentially over recent years. At the current rate of progress, the prospects for on-chip resonators operating past 10 GHz with *Q*'s >10,000 are not unreasonable in the next three years.

Micromechanical Signal Processors

As has been the case for transistors, a single micromechanical element is limited in the functions it can realize, and it is only after many micromechanical elements are combined into a complex circuit when the true functional breadth of this technology can be seen. In effect, vibrating RF MEMS elements are best viewed as circuit building blocks, that can be combined to achieve functions better tailored to a given purpose. Given that the property that allows transistors to be combined into large circuits is essentially their large gain, it follows that mechanical elements can be combined into equally large circuits by harnessing their large *Q*. As a simple example, transistor elements can be cascaded in long chains, because their gains compensate for the noise and other losses that would otherwise degrade the signal as it moves down the chain. On the other hand, mechanical elements can be cascaded into long chains because of their extremely low loss—a result of their high *Q*. In essence, if an element has an abundance of some parameter, then this can generally be used to build circuits of that element.

Being a general circuit technology, micromechanics can realize virtually any function that transistors can realize, including amplification [15]. However, they are perhaps at their best (i.e., most efficient) when performing frequency processing, which makes them ideal for communications applications. As such, some of the most compelling applications of micromechanical circuits include frequency selection (e.g., via micromechanical filters) and low power frequency generation (i.e., oscillators), using a combination of micromechanical resonators and transistor sustaining and controlling circuits.

A. Low-Loss Tiny-Bandwidth Micromechanical Filters

Fig. 6(a) presents a generalized schematic describing the basic topology used by the vast majority of bandpass frequency fil-

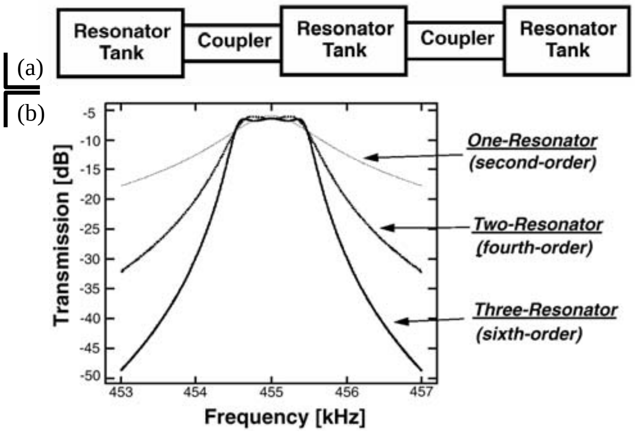

Fig. 6: (a) Basic topology of a bandpass filter. (b) Filter response simulations clearly showing sharper passband-to-stopband roll-offs as the number of resonators used increases.

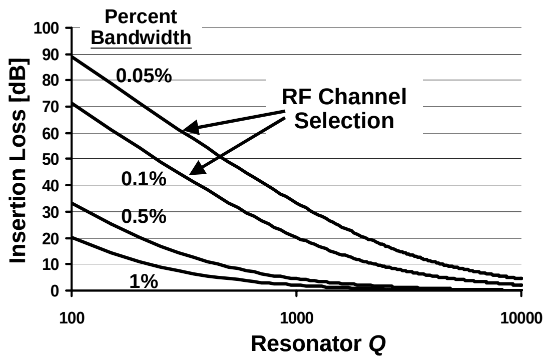

Fig. 7: Plot of insertion loss versus *Q* with percent bandwidth as a third variable for a four-resonator Chebyshev filter with 0.01% ripple.

ters to date. As shown, such filters are often comprised of a number of bandpass biquad resonators linked by some sort of coupling element to form a coupled network. As shown in Fig. 6(b), the larger the number of resonators used, the sharper the transition from the passband to the stopband, and the more effective the filter. In ladder filter synthesis, the resonators might be *LC* tank circuits, and the coupling elements either inductors or capacitors or both, depending upon whether the implementation is parallel or series, respectively, and depending on the filter bandwidth (i.e., narrow or wide) [16].

Filters are at their best when the circuit elements that comprise them exhibit very high *Q*. In particular, it is the *Q*'s of its constituent elements that determine the insertion loss (and thus, noise figure) of any filter in the transmit or receive chain of a wireless RF front-end; the higher the *Q* of its constituent elements, the lower the insertion loss, hence, the lower the noise figure contribution from the filter in question. To illustrate, Fig. 7 presents a plot of insertion loss versus resonator *Q* with percent bandwidth as a third variable, for a four-resonator Chebyshev filter with 0.01% ripple. Clearly, the insertion loss is a strong function of both *Q* and percent bandwidth, decreasing with increases in *Q*, and increasing with decreases in percent bandwidth. From Fig. 7, to maintain an insertion loss less than 4dB, an RF channel-select filter for PCS 1900 requiring a (1.25/1900)=0.066% bandwidth would require constituent

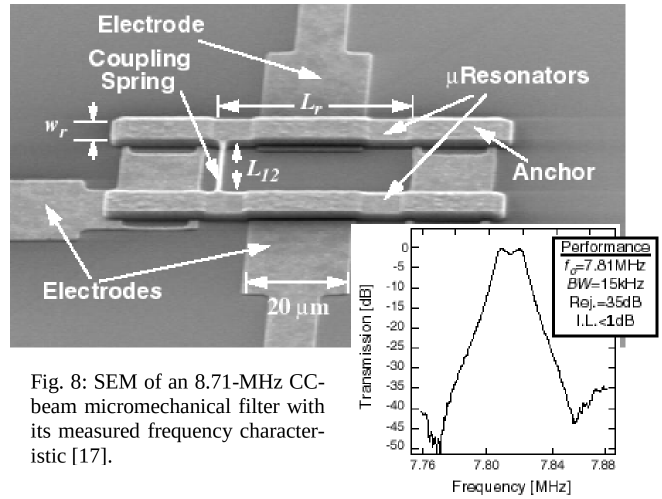

Fig. 8: SEM of an 8.71-MHz CC-beam micromechanical filter with its measured frequency characteristic [17].

resonators with *Q*'s >10,000—a figure not achievable via previous off-chip resonator technologies, including *LC* tanks, SAW's, crystals, and FBAR's, but now achievable via on-chip micromechanical resonator technology.

To construct a micromechanical filter, the general topology of Fig. 6 can be used with each resonator tank replaced with a vibrating micromechanical resonator. Although the coupling links can still be *L*'s and/or *C*'s, much better performance can be obtained by staying completely in the mechanical domain and using mechanically vibrating coupling links. Fig. 8 presents the SEM of an 8.71-MHz pure micromechanical filter utilizing two clamped-clamped beam resonators linked by a flexural-mode coupling beam, along with a measured frequency characteristic. By avoiding the use of electrical elements in the filter structure, this purely mechanical filter benefits from better resilience against substrate feedthrough interference, which can no longer directly interfere with the purely mechanical operation of the filter. With resonator *Q*'s of 6,000, this filter exhibits a measured insertion loss of less than 1dB for a 0.2% bandwidth [17].

To emphasize the circuit nature of the mechanical structure in Fig. 8, Fig. 9 presents its equivalent electrical circuit network, where each mechanical structure is modeled by an equivalent circuit, much like small-signal circuits for transistors. Here, each resonator is modeled by an *LCR* tank, with values for the *L*, *C*, and *R*, equal to the effective mass, stiffness, and damping, of the resonator, respectively. Since the coupling beam actually behaves like a mechanical transmission line, it is modeled by a T-network of energy storage elements, similar to the model for an electrical transmission line. The specific locations where the coupling beam attaches to each resonator actually determine the bandwidth of the filter structure, so also must be modeled. The turns ratios of the transformers flanking the coupling beam T-network do just this. To complete the model, two more transformers are used to model the capacitive electromechanical transducers at the input and output ports.

As previously mentioned, even better filter performance can be attained by using a larger number of resonators. To this end, a three-resonator micromechanical filter utilizing lower frequency folded-beam resonators [5] (as a conservative measure

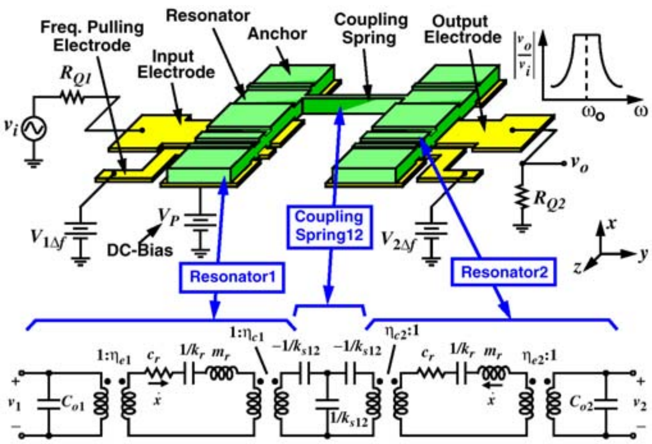

Fig. 9: Detailed schematic of the micromechanical filter of Fig. 8, showing the needed bias, excitation, and termination elements, and equating it to an electrical equivalent circuit [17].

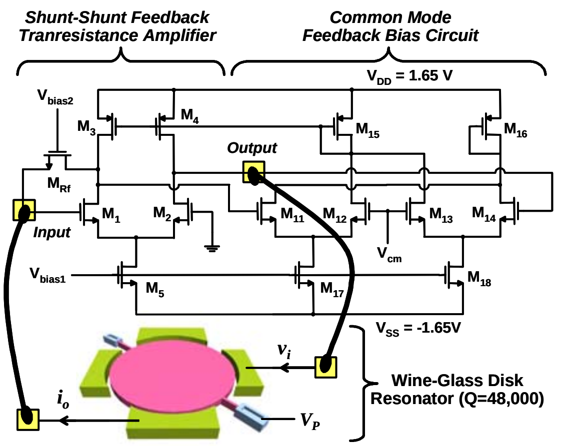

Fig. 10: Circuit schematic of a 61-MHz series resonant reference oscillator using a wine-glass disk resonator frequency-setting element with a Q of 48,000 in vacuum, and 10,000 in air [25].

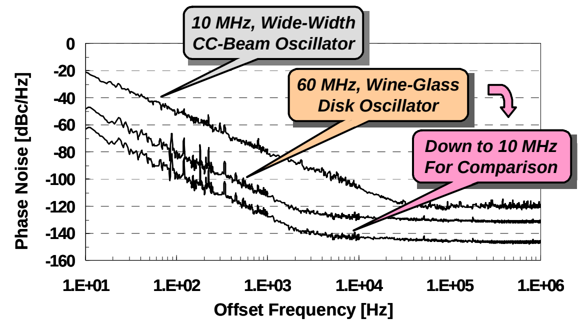

Fig. 11: Measured phase noise density versus carrier offset for the 10-MHz CC-beam oscillator of [24] and the 60-MHz wine-glass oscillator of [25], with an extrapolation for the latter down to 10 MHz for fair comparison.

for this first 3-resonator implementation) and flexural-mode couplers has been demonstrated [18]. With folded-beam resonator Q's exceeding 30,000, this filter achieves an impressive insertion loss of less than 0.6 dB for a tiny percent bandwidth of only 0.09%, which is on the order of what is needed for RF channel-selection. And all this with a 20 dB filter shape factor of only 1.70 and a stopband rejection of 64 dB. If this kind of performance can be duplicated at RF frequencies, then on-chip RF channel-selection, and all of its associated power and robustness advantages, could become a reality.

B. Ultra-Stable Local Oscillators

The local oscillator (LO) represents another key function in a communication circuit where resonator Q contributes substantially to performance. In particular, the Q of the frequency-setting tank used in any oscillator essentially sets the long- and short-term stability of its frequency output. For example, if the Q of the resonator tank is less than about 1,000, then the temperature stability of the overall oscillator would be determined primarily by that of the sustaining amplifier circuit, which is usually quite bad—nowhere near the needs of wireless communications. On the other hand, if the resonator tank is greater than ~1,000, then the resonator tank governs the oscillator temperature dependence—a much better situation, given that the quartz crystal blanks presently used have orders of magnitude smaller temperature dependencies than transistor circuits, on the order of 35 ppm (uncompensated) over 0-70^{o}C, and much better (~2 ppm) with active compensation [19]. As a reminder, this is one of the primary reasons why present-day LO's generally consist of VCO's locked to quartz crystal reference oscillators; the crystal reference provides the needed temperature stability (as well as the needed close-to-carrier phase noise). Given that micromechanical resonators have now been demonstrated with temperature dependencies on par with (and arguably better than) quartz crystals [20], high Q micromechanical resonators are expected to retain the temperature stability advantages of quartz when used in oscillators.

For the case of short-term stability, tank Q often plays an even bigger role in governing the close-to-carrier phase noise of any oscillator. In particular, the oscillator phase noise density L as a function of frequency offset f_m from the carrier f_o can often be approximated by Leeson's equation [23]

$$L(f_m) = \frac{FkT}{2P_{av}}\left[1+\frac{f_c}{f_m}+\left(\frac{f_o}{2Q_L f_m}\right)^2\left(1+\frac{f_c}{f_m}\right)\right] \quad (3)$$

where Q_L is the loaded Q; F and f_c are the noise factor and flicker corner frequency, respectively, of the active device; P_{av} is the average power through the resonator; k is the Boltzmann constant; and T is temperature. (3) clearly shows an inverse square law dependence on Q, suggesting that phase noise goes down in a hurry when the loaded Q of the resonator tank goes up. Given that the micromechanical disk and ring resonators of rows 4 and 5 of Table 1 have posted the highest room temperature Q's of any on-chip resonator above 1 GHz to date, the use of MEMS technology in compact LO implementations is fully expected to yield substantial improvements in LO performance. In particular, according to Leeson's equation, if a present-day VCO attains -121 dBc/Hz at a 600 kHz offset from an 1.8 GHz carrier using an LC tank with a Q of 30, then the use of a vibrating micromechanical disk resonator with a Q of 10,000 should provide ~50 dB of improvement, or -171 dBc/Hz at a 600 kHz carrier offset.

If phase noise this good is not needed in a particular application, then the oscillator carrier power can be further lowered until the phase noise matches the needed performance—a strategy that takes advantage of the Q versus power trade-off clearly seen in (3), and just one of many instances of this kind of trade-off in communications. In fact, much of the incentive for the use of high-Q MEMS circuits in future communication systems revolves around this Q versus power trade-off, where the more high-Q elements used and the higher their Q, the lower the power consumption and better the robustness of a given transceiver design.

To date, work towards demonstrating the above GHz oscillator using a micromechanical resonator tank is ongoing. However, a lower frequency reference oscillator based on a 61-MHz wine-glass-mode cousin of the disk resonator (row 3 of Table 1 [21]) was recently published that consumed 950μW of power towards phase noise marks at 1kHz and far-from-carrier offsets of -110 and -132 dBc/Hz, respectively [25]. Fig. 10 and Fig. 11 present the circuit schematic and measured phase noise plot, respectively, for this oscillator. As indicated in the plot, when translated down to 10MHz for fair comparison, these values equate to -125 and -145, respectively [25], both of which satisfy or nearly satisfy (depending on who you talk to) the needs of GSM cellular phones. With a resonator Q of 48,000, this oscillator was actually expected to perform much better, even when operating with such low power consumption. Unfortunately, however, an unexpected $1/f^3$ noise component introduced itself at close-to-carrier offsets, most likely caused by resonator nonlinearities involved in the oscillation amplitude limiting process. Other work [26] indicates that this $1/f^3$ component can be removed (leaving the expected $1/f^3$) by designing so that limiting occurs through transistor circuit nonlinearity, not resonator nonlinearity. It is expected that this will be easier to do at GHz frequencies, since higher frequency resonators are stiffer and can handle larger powers than the medium frequency wine-glass disk of Fig. 10.

Remaining Issues

Although Q is arguably the most important parameter governing the performance of the above filter and oscillator applications, it is by no means the only important one. Other very important characteristics that likely will ultimately determine the application range of vibrating RF MEMS include temperature and aging stability, power handling, and impedance.

A. Temperature and Aging Stability

As already mentioned, with the right design, the temperature stability of a micromechanical resonator can be on par with that of an AT-cut quartz crystal. Such a statement, on the other hand, cannot yet be made with regard to aging or drift. Although initial data seems to indicate an aging characteristic similar to that for quartz, where a fast initial frequency change is followed by slow movement to a flat asymptote, the jury is still out on the aging stability of micromechanical resonator devices, especially for applications as stringent as oscillators, where less than 3 ppm per year frequency shift is required. To more fully characterize these devices in this regard, methods for accelerated aging tests are needed. With recent efforts to commercialize micromechanical resonator technology, data on aging should be forthcoming over the next year or so [27].

B. Out-of-Band Power Handling

As modeled in [28], the power handling ability and linearity of micromechanical resonators improve with frequency, mainly because these devices generally become stiffer as their frequencies increase. For example, using [29]'s formula for the third-order intercept point IIP_3 for a capacitively transduced micromechanical resonator hit with interferers at 200kHz and 400kHz offsets, the IIP_3 of -3dBm for a 1,500 N/m stiff 9.2-MHz CC-beam pales in comparison to the >35dBm typical of the 1.5-GHz radial-mode disk in row 4 of Table 1, which has a much higher stiffness of ~10^8 N/m.

C. Impedance and In-Band Power Handling

For the case of micromechanical filters (but not oscillators), the remaining issues most responsible for hesitation among potential users is the larger-than-conventional impedances so far presented by these devices and, for transmit applications, their limited in-band power handling ability, both of which are related. (Note that in-band power handling for receive applications is already sufficient.) Although micromechanical resonators with series motional impedances (R_x's) lower than 50Ω have been demonstrated [25][24], the majority of vibrating RF MEMS devices work more comfortably with R_x's values that lead to filter termination impedances much larger than the 50-370Ω often desired by standard antennas. This is especially true when considering that the actual termination impedance required by a low loss micromechanical filter will be on the order of 10X its end resonator R_x's.

From (2), it should be clear that smaller impedances are readily achievable as long as electrode-to-resonator gap spacings can be made as small as needed, or the electrode-to-resonator bias voltage can be made as large as needed. Unfortunately, the gap spacing cannot be infinitely small, nor can the bias voltage be infinitely large. While there are certainly physical limitations governed by technology, a more fundamental limitation involves a trade-off between impedance, governed by (2), and linearity, governed by the IIP_3 expression in [29]. In particular, the smaller the gap spacing and the larger the bias voltage, the smaller the R_x, but also the smaller the IIP_3.

If gap spacing and bias voltage are not options, then perhaps the next easiest parameter to adjust towards lower motional resistance is the electrode-to-resonator overlap area A, which under the right conditions can have a stronger influence on R_x than IIP_3, so would make for a more favorable change. The ring in row 5 of Table 1 has an advantage in this regard, since its frequency depends mainly on the width of its structure, and not its radius. This means the ring can be made as large as needed to achieve as large an A as needed, while retaining the same frequency, as is done by example in [12].

On the other hand, a similar (perhaps bigger) increase in A could also be attained by summing the perimeter areas of enough radial-mode disk resonators that would fit within the total area inside such an enlargened ring. To match the frequencies of the resonators in such an array, coupling links can be inserted between resonators to form a coupled array (much like a filter) in which all individual resonator responses automatically combine into a single vibration mode at a specific mode frequency, allowing perfect summation of resonator outputs, no matter how large the array [30]. The use of an array of resonators to match the impedance of a micromechanical circuit to a macroscopic element (e.g., an antenna) is really no different from the use of a cascade of progressively larger inverters to allow a minimum-sized digital gate to drive an off-chip board capacitor. In essence, micro (or nano) scale circuits prefer to operate with higher impedances than macro-scale ones, and interfacing one with the other requires a proper impedance transformation. In a building block circuit environment, such an impedance transformation is most conveniently accomplished via large numbers of circuit elements, whether they be electronic transistors or mechanical resonators.

Conclusions

Vibrating RF MEMS technology has now reached frequencies required for critical RF functions in wireless applications and has done so with previously unavailable on-chip *Q*'s exceeding 10,000. *Q*'s this high may now encourage paradigm-shifting communication architectures that can eliminate interferers immediately after the antenna, allowing subsequent electronics to operate with much lower dynamic range and power consumption than would otherwise be needed. Given present transistor scaling trends towards lower dynamic range digital devices, such a relaxation in dynamic range requirements may be arriving at an opportune time. In addition, if RF channel-selection becomes available, there is even the possibility of eliminating altogether the "analog RF front end" as we know it, and go straight to digital after the antenna. Such an approach, if combined with sub-sampling methods, could be instrumental in achieving power consumptions low enough to achieve truly unattended sensor networks. Indeed, the possibilities for micromechanical circuits are endless. Before any of these can become reality, however, a number of key issues (e.g., impedance, drift stability, transistor integration) must be resolved. Work pursuant to this is ongoing.

Acknowledgment. This work was supported under the DARPA NMASP Program and by the NSF ERC in WIMS.

References

[1] A. A. Abidi, "Direct-conversion radio transceivers for digital comms," *IEEE J. Solid-State Circuits*, vol. 30, No. 12, pp. 1399-1410, Dec. 1995.
[2] C.P. Yue and S.S. Wong, "On-chip spiral inductors with patterned ground shields for Si-based RF IC's," *IEEE Journal of Solid-State Circuits*, vol. 33, no. 5, pp.743-752, May 1998.
[3] C. T.-C. Nguyen, "Transceiver front-end architectures using vibrating micromechanical signal processors (invited)," *Dig. of Papers*, Topical Meeting on Silicon Monolithic Integrated Circuits in RF Systems, Sept. 12-14, 2001, pp. 23-32.
[4] C. T.-C. Nguyen, "Transceiver front-end architectures using vibrating micromechanical signal processors," chapter in *RF Technologies for Low Power Wireless Communications*, edited by G. I. Haddad, T. Itoh, and J. Harvey, pp. 411-461. New York: Wiley IEEE-Press, 2001.
[5] C. T.-C. Nguyen and R. T. Howe, "An integrated CMOS micromechanical resonator high-*Q* oscillator," *IEEE J. Solid-State Circuits*, vol. 34, no. 4, pp. 440-455, April 1999.
[6] K. Wang, A.-C. Wong, and C. T.-C. Nguyen, "VHF free-free beam high-*Q* micromechanical resonators," *IEEE/ASME J. Microelectromech. Syst.*, vol. 9, no. 3, pp. 347-360, Sept. 2000.
[7] M. U. Demirci and C. T.-C. Nguyen, "Higher-mode free-free beam micromechanical resonators," *Proceedings*, 2003 IEEE Int. Frequency Control Symposium, Tampa, Florida, May 5-8, 2003, pp. 810-818.
[8] X. M. H. Huang, C. A. Zorman, M. Mehregany, M. L. Roukes, "Nanodevice motion at microwave freqs," *Nature*, vol. 421, pg. 496, Jan. 30, 2003
[9] J. R. Vig and Y. Kim, "Noise in microelectromechanical system resonators," *IEEE Trans. Utrason. Ferroelec. Freq. Contr.*, vol. 46, no. 6, pp. 1558-1565, Nov. 1999.
[10] J. Wang, Z. Ren, and C. T.-C. Nguyen, "Self-aligned 1.14-GHz vibrating radial-mode disk resonators," *Dig. of Tech. Papers*, Transducers'03, Boston, Massachusetts, June 8-12, 2003, pp. 947-950.
[11] J. Wang, J. E. Butler, T. Feygelson, and C. T.-C. Nguyen, "1.51-GHz polydiamond micromechanical disk resonator with impedance-mismatched isolating support," *Proceedings*, 17th Int. IEEE MEMS Conf., Maastricht, The Netherlands, Jan. 25-29, 2004, pp. 641-644.
[12] S.-S. Li, Y.-W. Lin, Y. Xie, Z. Ren, and Clark T.-C. Nguyen, "Micromechanical Hollow-Disk Ring Resonators," *Proceedings*, 17th Int. IEEE MEMS Conf., Maastricht, Netherlands, Jan. 25-29, 2004, pp. 821-824.
[13] B. Bircumshaw, G. Lui, H. Takeuchi, T.-J. King, R. T. Howe, O. O'Reilly, and A. P. Pisano, "The radial bulk annular res.: towards a 50Ω MEMS filter," *Dig. of Tech. Papers*, Transducers'03, Boston, Massachusetts, June 8-12, 2003, pp. 875-878.
[14] Y. Xie, S.-S. Li, Y.-W. Lin, Z. Ren, and C. T.-C. Nguyen, "UHF Micromechanical Extensional Wine-Glass Mode Ring Resonators" *Technical Digest*, 2003 IEEE International Electron Devices Meeting, Washington, DC, Dec. 8-10, 2003, pp. 953-956.
[15] J. P. Raskin, A. R. Brown, B. T. Yakub, and G. M. Rebeiz, "A novel parametric-effect MEMS amplifier," *IEEE/ASME J. Microelectromech. Syst.*, vol. 9, no. 4, pp. 528-537, Dec. 2000.
[16] A. I. Zverev, *Handbook of Filter Synthesis*. New York: John Wiley & Sons, 1967.
[17] F. D. Bannon III, J. R. Clark, and C. T.-C. Nguyen, "High frequency micromechanical filters," *IEEE J. Solid-State Circuits*, vol. 35, no. 4, pp. 512-526, April 2000.
[18] K. Wang and C. T.-C. Nguyen, "High-order medium frequency micromechanical electronic filters," *IEEE/ ASME J. Microelectromech. Syst.*, vol. 8, no. 4, pp. 534-557, Dec. 1999.
[19] M. E. Frerking, *Crystal Oscillator Design and Temperature Compensation*. New York: Van Nostrand Reinhold, 1978.
[20] W. -T. Hsu and C. T. -C. Nguyen, "Stiffness-compensated temperature-insensitive micromechanical resonators," *Tech. Digest*, 2002 IEEE Int. MEMS Conf., Las Vegas, Nevada, Jan. 20-24, 2002, pp. 731-734.
[21] M. A. Abdelmoneum, M. U. Demirci, and C. T.-C. Nguyen, "Stemless wine-glass-mode disk micromechanical resonators," *Proceedings*, 16th Int. IEEE MEMS Conf., Kyoto, Japan, Jan. 19.-23, 2003, pp. 698-701.
[22] S. Pourkamali and F. Ayazi, "SOI-based HF and VHF single-crystal Si resonators with sub-100 nm vertical capacitive gaps, *Dig. of Tech. Papers*, Transducers'03, Boston, Massachusetts, June 8-12, 2003, pp. 837-840.
[23] D. B. Leeson, "A simple model of feedback oscillator noise spectrum," *Proc. IEEE*, vol. 54, pp. 329-330, Feb. 1966.
[24] Y.-W. Lin, S. Lee, Z. Ren, and C. T.-C. Nguyen, "Series-resonant micromechanical resonator oscillator," *Technical Digest*, 2003 IEEE Int. Electron Devices Mtg, Washington, DC, Dec. 8-10, 2003, pp. 961-964.
[25] Y.-W. Lin, S. Lee, S.-S. Li, Y. Xie, Z. Ren, and C. T.-C. Nguyen, "60-MHz wine glass micromechanical disk reference oscillator," *Digest of Technical Papers*, 2004 IEEE International Solid-State Circuits Conference, San Francisco, California, Feb. 15-19, 2004, pp. 322-323.
[26] S. Lee and C. T.-C. Nguyen, "Influence of automatic level control on μmechanical resonator oscillator phase noise," *Proceedings*, 2003 IEEE Int. Freq. Control Symp, Tampa, Florida, May 5-8, 2003, pp. 341-349.
[27] Personal communications with Discera, Inc.
[28] C. T.-C. Nguyen, "Frequency-selective MEMS for miniaturized low-power communication devices (invited)," *IEEE Trans. Microwave Theory Tech.*, vol. 47, no. 8, pp. 1486-1503, Aug. 1999.
[29] R. Navid, J. R. Clark, M. Demirci, and C. T.-C. Nguyen, "Third-order intermodulation distortion in capacitively-driven CC-beam micromechanical resonators," *Technical Digest*, 14^{th} Int. IEEE MEMS Conf, Interlaken, Switzerland, Jan. 21-25, 2001, pp. 228-231.
[30] M. U. Demirci, M. A. Abdelmoneum, and C. T.-C. Nguyen, "Mechanically corner-coupled square microresonator array for reduced series motional resistance," *Dig. of Tech. Papers*, Transducers'03, Boston, Massachusetts, June 8-12, 2003, pp. 955-958.